Available online at www.sciencedirect.com
SCIENCE DIRECT®
Optical Materials 28 (2006) 255–258
OPTICAL Materials
www.elsevier.com/locate/optmat

Spectroscopic properties of tungsten–tellurite glasses doped with Er^{3+} ions at different concentrations

Yongshi Luo [a], Jiahua Zhang [a,*], Jiangting Sun [a], Shaozhe Lu [a], Xiaojun Wang [a,b,*]

[a] Key Laboratory of Excited State Processes, Changchun Institute of Optics, Fine Mechanics and Physics, Graduate School of the Chinese Academy of Sciences, 16 Eastern South Lake Road, Changchun 130033, PR China
[b] Department of Physics, Georgia Southern University, Statesboro, GA 30460, USA

Received 23 September 2004; accepted 15 December 2004
Available online 8 February 2005

Abstract

Infrared spectra and lifetimes of $^4I_{13/2}$ state of Er^{3+} in tungsten–tellurite glasses doped with different concentrations of Er_2O_3 were measured and studied. Judd–Ofelt analysis on absorption spectra was performed. The lifetime of the $^4I_{13/2}$ state decreases with the increase of the Er^{3+} concentration due to energy transfer processes. The energy transfer coefficient of 1.6×10^{-18} cm^3 s^{-1} was obtained. It is observed that the nonradiative relaxation rate of $^4I_{11/2}$–$^4I_{13/2}$ transition of Er^{3+} in tungsten–tellurite glass is unchanged with the increase of Er^{3+} concentration, and about twice as that in TeO_2–ZnO–Na_2O glass.

PACS: 42.70.C; 78.20.C; 81.05.Pj; 74.25.Gz

Keywords: Erbium; Glasses; Nonradiative decay

1. Introduction

In order to increase the transmission capacity in wavelength division multiplexing (WDM) systems, many glass matrices [1–3] have been investigated extensively to obtain an intrinsically broader gain bandwidth than silica matrix for Er^{3+}-doped fiber amplifier (EDFA). Compared with silica, Er^{3+}-doped tellurite glass [4] has a broader emission band at 1.5 μm and a larger stimulated emission cross-section. A tellurite glass based fiber with 76 nm flat gain bands was reported in 1997 [5]. In addition, Er^{3+} solubility in tellurite glass is better than that in silica, making it possible to have a higher doping level. However, as a host for EDFA, tellurite glass has some drawbacks. First, the softening point of tellurite glass is 290 °C, which makes it liable to thermal damage at high optical intensities. Second, the phonon energy of the glass is about 770 cm^{-1}, which leads to a $^4I_{11/2}$–$^4I_{13/2}$ nonradiative relaxation rate too slow to allow pumping at 980 nm. To overcome those drawbacks, different compound tellurite based glasses have been investigated [6–9], including a tellurite–tungsten (TW) based glass. Tungsten–tellurite glass has the advantages of higher phonon energy, higher softening point, and a significantly broadened emission at 1.5 μm [9,10].

In this paper, we report the effect of Er^{3+} concentration on optical properties of Er^{3+} doped tungsten–tellurite glass. Nonradiative processes for $^4I_{11/2}$–$^4I_{13/2}$ and $^4I_{13/2}$–$^4I_{15/2}$ transition of Er^{3+}, J–O intensity parameters and 1.5 μm emission bandwidth are mainly studied. The quenching rate of $^4I_{13/2}$–$^4I_{15/2}$ transition obtained in TW

* Corresponding authors. Address: Key Laboratory of Excited State Processes, Changchun Institute of Optics, Fine Mechanics and Physics, Chinese Academy of Sciences, 16 Eastern South Lake Road, Changchun 130033, PR China. Tel./fax: +86 431 617 6317 (J.Zhang).
E-mail address: zjiahua@public.cc.jl.cn (J. Zhang).

0925-3467/$ - see front matter © 2005 Elsevier B.V. All rights reserved.
doi:10.1016/j.optmat.2004.12.013

glass is about 1.6×10^{-18} cm^3 s^{-1}, giving an upper-limit for doping concentration of Er^{3+} ions in TW glass.

2. Experimental

Two types of Er^{3+}-doped glass, (1) $(40 - 0.4x)TeO_2$–$(40 - 0.4x)WO_3$–$(20 - 0.2x)Li_2O$–xEr_2O_3 ($x = 0.1$–10) (TW glass) and (2) $70TeO_2$–$20ZnO$–$10Na_2O$–0.5% Er_2O_3, (TZN glass) were prepared using the conventional melting and quenching method.

Well-mixed powder in a crucible was melted at 750–900 °C for 0.5 h, then was quenched into a preheated brass mold to form glass. The quenched sample is annealed around the glass transition temperature for 2 h. The obtained glass samples were cut and polished into $10 \times 10 \times 2.0$ mm^3 size.

Emission spectra in the range of 900–1700 nm were measured using a TRIAX 550 spectrometer with spectral resolution of 1 nm under the excitation of 808 nm from a diode laser. Absorption spectra were measured using a UV-3101PC spectrometer. The lifetime of the $^4I_{13/2}$ state for Er^{3+} was measured with a 500 MHz Tektronix digital oscilloscope model TDS 3052 under excitation of 808 nm light pulses from an Optical Parametric Oscillator (Sunlite 8000). All the measurements were taken at room temperature.

3. Results and discussion

3.1. Infrared emission spectra of Er^{3+}

Fig. 1 shows the $^4I_{11/2}$–$^4I_{15/2}$ and $^4I_{13/2}$–$^4I_{15/2}$ emission spectra of Er^{3+} in $(40 - 0.4)TeO_2$–$(40 - 0.4x)WO_3$–$(20 - 0.2x)Li_2O$–xEr_2O_3 ($x = 0.1$–10) glasses doped with Er_2O_3 at different concentrations. It can be seen that the $^4I_{13/2}$–$^4I_{15/2}$ emission at 1.5 μm becomes broader as Er^{3+} concentration increases. The values of full-width-at-half-maximum (FWHM) of the emission peak ranges from 65 to 110 nm. This suggests that local environment becomes disordered with the increase of Er^{3+} doping level, broadening the Er^{3+} emission band at 1.5 μm. Furthermore, the integrated intensity ratio of the 1.5 μm band to the 0.98 μm band decreases as Er^{3+} concentration increases, as shown in Fig. 1. This ratio is governed by $^4I_{11/2}$–$^4I_{13/2}$ nonradiative relaxation and lifetime of $^4I_{13/2}$ state, which will be studied in detail in the following sections.

3.2. Judd–Ofelt analysis on absorption spectra of the TW glass

Fig. 2 shows the absorption spectra of the TW glasses. The absorption spectra consist of seven absorption bands peaked at 1527, 975, 796, 652, 541, 520 and 488 nm, corresponding to the Er^{3+} transitions from the ground state $^4I_{15/2}$ to the excited states $^4I_{13/2}$, $^4I_{11/2}$, $^4I_{9/2}$, $^4F_{9/2}$, $^4S_{3/2}$, $^2H_{11/2}$ and $^4F_{7/2}$, respectively. Some optical properties are directly related to Judd–Ofelt (J–O) parameters, which can be obtained by analyzing absorption spectra using J–O theory [11,12]. From the theory, the strength of electric dipole transition between two J states, S_{ed} can be expressed,

$$S_{ed}(J;J') = \sum_{t=2,4,6} \Omega_t \langle \alpha SL, J \| U^{(t)} \| \alpha' S' L', J' \rangle^2 \quad (1)$$

where Ω_t ($t = 2$, 4, and 6) is the Judd–Ofelt parameter, αSL define the other quantum numbers of the states, and the ($\| U^{(t)} \|$) is doubly reduced matrix element of unit

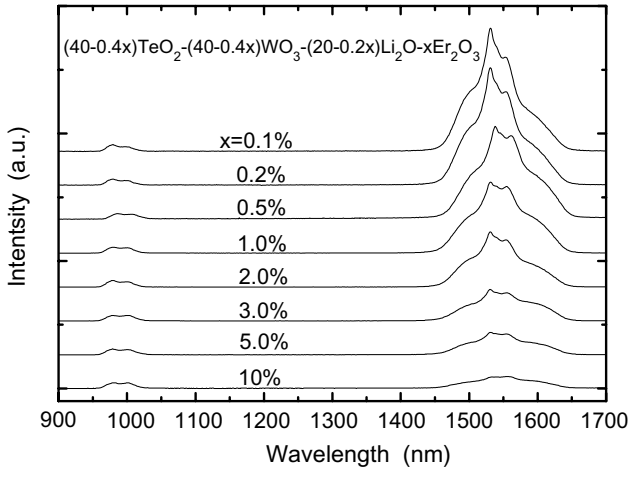

Fig. 1. Emission spectra from $^4I_{11/2}$–$^4I_{15/2}$ and $^4I_{13/2}$–$^4I_{15/2}$ transitions of Er^{3+} in $(40 - 0.4x)TeO_2$–$(40 - 0.4x)WO_3$–$(20 - 0.2x)Li_2O$–xEr_2O_3 ($x = 0.1$–10) glasses. The $^4I_{11/2}$–$^4I_{15/2}$ emission bands are normalized to the one for Er_2O_3 concentration of 0.1 mol%.

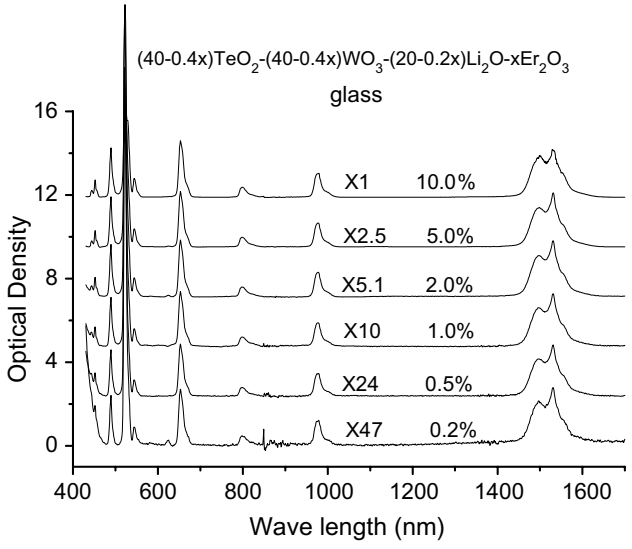

Fig. 2. Absorption spectra of TW glasses doped with different concentration of Er_2O_3.

Table 1
J–O parameters and radiative transition rates calculated from the absorption spectra

Glass	Ω_2 10^{-20}	Ω_4 10^{-20}	Ω_6 10^{-20}	A_{10} (s^{-1}) ($^4I_{13/2}$–$^4I_{15/2}$)	A_{20} (s^{-1}) ($^4I_{11/2}$–$^4I_{15/2}$)	A_{21} (s^{-1}) ($^4I_{11/2}$–$^4I_{13/2}$)	τ_{1r} ($^4I_{13/2}$) (ms)	τ_{2r} ($^4I_{11/2}$) (ms)
TW0.2%	7.99	1.71	1.22	243.86	362.22	44.87	4.1	2.46
TW0.5%	7.79	1.61	1.20	238.84	344.60	42.60	4.2	2.58
TW1.0%	7.77	1.72	1.20	240.28	344.30	43.03	4.2	2.58
TW2.0%	7.15	1.56	1.28	249.87	351.53	43.89	4.0	2.53
TW5.0%	6.06	1.65	1.21	245.97	334.49	43.24	4.1	2.56
TW10%	6.58	1.72	1.20	252.35	346.35	44.48	4.0	2.56
TZN0.5%	5.88	1.41	1.13	220.2	304.51	38.59	4.5	2.91

tensor operator calculated in the intermediate coupling approximation. The Ω_t parameters can be obtained from a least-squares fit of Eq. (1) to the line strength of the absorption bands mentioned above. Absorption data and fitting results are listed in Table 1.

Parameter Ω_2 monotonically decreases with the increase of Er^{3+} concentration, as shown in Table 1, while Ω_4, and Ω_6 have no significant change when the concentration increases. In general, local structure around the doped ions in the host has a strong effect on J–O parameters. Parameter Ω_2 is affected by the covalent bonding and parameters Ω_4 and Ω_6 are related to the rigidity of the medium where the ions are situated. Thus the experimental results suggest that the covalent bond the Er–O becomes weaker as Er^{3+} concentration increases in TW glass.

3.3. Lifetime and concentration quenching of $^4I_{13/2}$ level

Fig. 3 represents the lifetimes (circles) and nonradiative transition rates (squares) of $^4I_{13/2}$ level of Er^{3+} in TW glass with different Er^{3+} concentrations. The lifetime of $^4I_{13/2}$ level decreases with the increase of Er^{3+} concentration, which can be attributed to the nonradiative relaxation. The rate of nonradiative transition linearly increases with the increase of Er^{3+} concentration, as shown in Fig. 3.

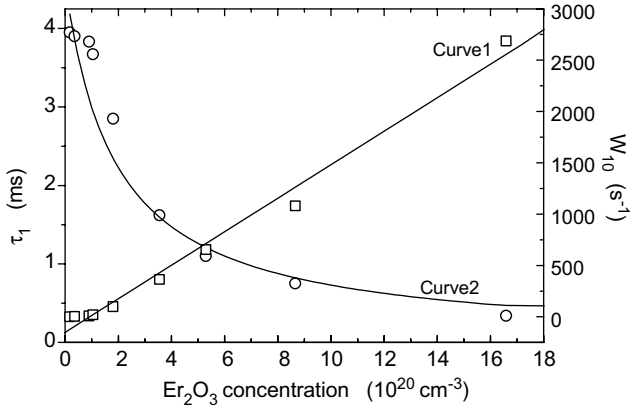

Fig. 3. Dependence of measured lifetimes (squares) and nonradiative decay rates (circles) of $^4I_{13/2}$ level of Er^{3+} on Er^{3+} concentrations in TW glasses. The solid curves 1 and 2 are calculated using $W_1 = kC + W_{MP}$ and $1/(kC + W_{MP} + A_{10})$, respectively.

The nonradiative relaxation rate (W_{10}) of $^4I_{13/2}$ level is obtained using the following equation,

$$W_{10} = \tau_1^{-1} - A_{10} \tag{2}$$

where τ_1 and A_{10} are lifetime (measured) and radiative transition rate (calculated) of $^4I_{13/2}$ level, respectively. The nonradiative relaxation rate consists of a multi-phonon relaxation rate (W_{MP}) and an energy transfer rate (W_{ET}) which is Er^{3+} concentration dependent. Energy transfer rate and Er^{3+} concentration can be described by a linear relationship, $W_{ET} = kC$, where k and C are energy transfer coefficient and Er^{3+} concentration, respectively. The value of k is determined to be 1.6×10^{-18} cm^3 s^{-1} in this work by fitting the experimental data (squares) with a linear function: $W_1 = kC + W_{MP}$, (curve 1). The curve 2 is given by $1/(kC + W_{MP} + A_{10})$. Both calculated solid curves, as shown in Fig. 3, fit the measured data very well.

3.4. The $^4I_{11/2}$–$^4I_{13/2}$ nonradiative relaxation rates in TW glass and TZN glass

Fig. 4 depicts a energy level diagram of Er^{3+} at low energy levels. When pumped by 808 nm diode laser, Er^{3+} is excited from ground state to $^4I_{9/2}$ level, which rapidly relaxes to $^4I_{11/2}$ state through nonradiative decay. Subsequently, the $^4I_{13/2}$ level is populated through $^4I_{11/2}$–$^4I_{13/2}$ nonradiative relaxation process. The rate of $^4I_{11/2}$–$^4I_{13/2}$ relaxation is very important for creating population inversion of $^4I_{13/2}$ level for optical amplification at 1.5 μm. In the steady excitation, one has

$$A_{21}n_2 + W_{21}n_2 = n_1/\tau_1 \tag{3}$$

where A_{21} is $^4I_{11/2}$–$^4I_{13/2}$ radiative transition rate, W_{21} is $^4I_{11/2}$–$^4I_{13/2}$ nonradiative relaxation rate, n_2 and n_1 is the population of $^4I_{11/2}$ and $^4I_{13/2}$ level respectively. If the intensity ratio of the 1.5 μm emission to the 0.98 μm emission is denoted by α, then

$$\alpha = A_{10}n_1/A_{20}n_2 \tag{4}$$

From Eqs. (3) and (4), we have

$$W_{21} = \alpha A_{21}/A_{10}\tau - A_{21} \tag{5}$$

where A_{21} can be neglected because of $W_{21} \gg A_{21}$, as reported in Ref. [6]. The $^4I_{11/2}$–$^4I_{13/2}$ nonradiative

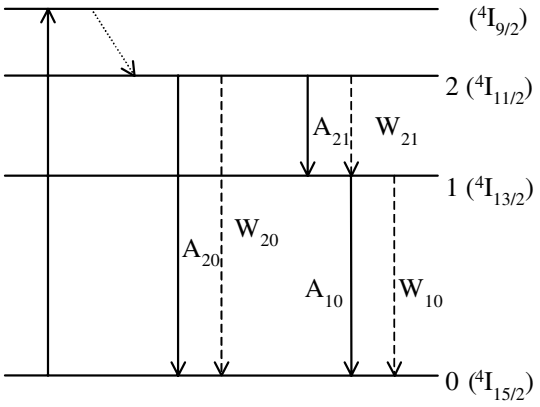

Fig. 4. An energy level diagram of Er^{3+} ions. The transition from $^4I_{15/2}$–$^4I_{9/2}$ indicates an optical transition under 808 nm excitation. Solid lines represent the radiative processes and dashed lines are the nonradiative processes.

relaxation rates W_{21} are then calculated using the data listed in Table 1, and the measured lifetime from Fig. 3, and Eq. (5). The rates are normalized to the one for the lowest Er^{3+} concentration in the TW glasses and are plotted in Fig. 5.

As indicated in Fig. 5, W_{21} increases slightly with the increase of Er^{3+} concentration. This is due to the domination of multiphonon decay in the $^4I_{11/2}$–$^4I_{13/2}$ nonradiative relaxation; the contribution from the energy transfer, which is concentration dependent, is neglectable, even in the case of high concentration of Er^{3+} doped TW glass. W_{21} for a TZN glass is also plotted in Fig. 5. It is observed that W_{21} for Er^{3+} doped TW glass is about twice as high as W_{21} for Er^{3+} doped TZN glass. Hence, population feeding of $^4I_{13/2}$ of Er^{3+} in TW glass is more effective than that in TZN glass under 0.98 μm pumping into the $^4I_{11/2}$ level of Er^{3+} ions.

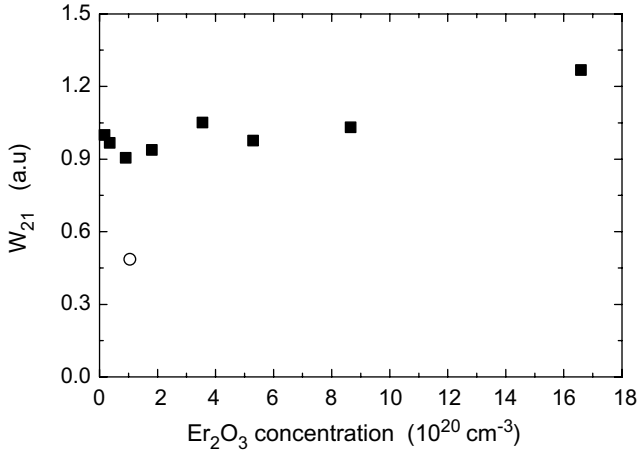

Fig. 5. The $^4I_{11/2}$–$^4I_{13/2}$ nonradiative relaxation rates against concentration. The rates (W_{21}) are normalized to the one for the least concentration (0.1 mol% Er_2O_3) in TW (square) and TZN (circle) glasses, respectively.

4. Conclusions

The 1.5 μm emission band becomes broader with increasing concentration of Er^{3+} ions in tungsten–tellurite glasses. The values of FWHM at 1.5 μm emission range from 65 to 110 nm. J–O analysis indicates that the covalency of the Er–O bond becomes weaker with the increase of Er^{3+} concentration in TW glasses. The lifetime of the $^4I_{13/2}$ state decreases with the increase of the Er^{3+} concentration due to energy transfer process. The energy transfer coefficient among $^4I_{13/2}$ states of different Er^{3+} ions in TW glass was determined to be 1.6×10^{-18} cm^3 s^{-1}. The nonradiative relaxation rate of $^4I_{11/2}$–$^4I_{13/2}$ transition of Er^{3+} in TW glass remains unchanged with the increase of Er^{3+} concentration, and is about twice as high as that in TeO_2–ZnO–Na_2O glass. Hence, population feeding of $^4I_{13/2}$ of Er^{3+} in TW glass is more effective than that in TZN glass under 980 nm pumping into the $^4I_{11/2}$ level of Er^{3+} ions.

Acknowledgements

The authors acknowledge the supports by the National Natural Foundation of China under Grant No. 90201010,50172047,10274083, the Natural Science Foundation of Jilin Province of China, under Grant No. 20030104, and "One Hundred Talents Program" of Chinese Academy of Sciences.

References

[1] D.R. MacFarlane, J. Javorniczky, P.J. Newman, V. Bogdanov, D.J. Booth, W.E.K. Gibbs, J. Non-Cryst Solids 213–214 (1997) 158.
[2] S. Tanabe, N. Sugimoto, S. Ito, et al., J. Lumin. 87–89 (2000) 670.
[3] R. Francini, F. Giovenale, U.M. Grassano, P. Laporta, S. Taccheo, Opt. Mater. 13 (4) (2000) 417.
[4] S. Tanabe, K. Suzuki, N. Soga, T. Hannada, J. Opt. Soc. Am. B. 11 (5) (1994) 933.
[5] A. Mori, Y. Ohishi, S. Sudo, Electron. Lett. 33 (1997) 863.
[6] X. Feng, S. Tanabe, T. Hanada, J. Am. Ceram. Soc. 84 (1) (2001) 165.
[7] R. Rolli, M. Mortagha, et al., Opt. Mater. 21 (2003) 743.
[8] S. Hocde, S.B. Jiang, et al., Opt. Mater. 25 (2) (2004) 149.
[9] S.X. Shen, Mira Naflaly, Aminesh Jha, Opt. Comm. 205 (2000) 101.
[10] R. El-mallawary, A. Patra, et al., Opt. Mater. 26 (3) (2004) 267.
[11] B.R. Judd, Phys. Rev. 127 (3) (1962) 750.
[12] G.S. Ofelt, J. Chem. Phys. 37 (3) (1962) 511.